ISSN 0036-0295, Russian Metallurgy (Metally), Vol. 2018, No. 12, pp. 1152–1160. © Pleiades Publishing, Ltd., 2018.
Original Russian Text © N.V. Abraimov, 2018, published in Elektrometallurgiya, 2018, No. 4, pp. 19–29.

HARDENING AND COATING TECHNOLOGIES

Combined Coatings for Gas Turbine Blades

N. V. Abraimov*

NPTs Gas Turbine Manufacture SALYUT, Moscow, Russia

**e-mail: diagnostika@salut.ru*

Received December 5, 2017

Abstract—The paper reports the results of studying the phase compositions of the metallic compounds that participate in the aluminum and chromium transfer from powders on the metal surface upon vacuum chromoaluminizing and the life characteristics of combined condensation-diffusion coatings containing Cr, Al, Ta, W, Hf, and Y. The presence of high-temperature metals in the sublayer of aluminide coatings is found to increase the life of the parts operating at temperatures up to 1100–1150°C substantially.

Keywords: chromoaluminizing, coating, alloys, oxidation

DOI: 10.1134/S0036029518120029

Vacuum chromoaluminizing is widely used to protect high-temperature nickel superalloys from gas corrosion [1–3]. In this case, the saturation of protected part surfaces with aluminum and chromium is carried out in powder mixtures at temperatures of 1000–1200°C.

The powder mixtures contain:

(i) aluminum, which is an active element;

(ii) chromium, which improves the protective properties of a coating and influences the aluminum activity in a mixture;

(iii) aluminum oxide used to prevent mixture sintering.

The proportion of aluminum and chromium in a metallic component determines the aluminum activity in a mixture.

To understand the mechanism of forming an aluminide coating and developing the technology of its deposition, it is necessary to know the phase composition of the powder mixtures used for chromoaluminizing. Knowing the phase composition, we can judge on the mixture activity. In this work, we study the phase compositions of the mixtures, the chemical compositions and the heat treatment regimes of which are presented in Table 1.

According to the Cr–Al phase diagram, we can assume that the mixture used in this work contain the following phases: the solid solution of aluminum in α-Cr chromium, Cr_2Al, Cr_5Al_8, Cr_4Al_9, and $CrAl_4$ [4]. These phases were identified using the ASTM database and reference tables.

Qualitative phase analysis of the mixtures was carried out on a DRON-4 X-ray diffractometer using Cu$K\alpha$ radiation and a monochromator (pyrolytic graphite) on the reflected beam. The change in the phase composition of the powder mixtures as the aluminum content increases is shown in Fig. 1, where the portions of the X-ray diffraction patterns in the angular range $2\theta = 20°–50°$ are shown. Figure 2 shows the

Table 1. Chemical and phase compositions of the powder mixtures for coatings and heat treatment regimes [11]

Content of components in powders, wt %			Heat treatment conditions	Powder phase composition
Al	Cr	Al_2O_3		
4	46	50	t = 1150°C, τ = 1 h 10 min, p = 0.2–0.14 Pa	α-Cr, Al_2O_3
8	42	50	″	α-Cr, Cr_2Al, Al_2O_3
12	38	50	″	Cr_2Al, Cr_5Al_8, Al_2O_3
15	35	50	″	″
18	32	50	″	″
24	26	50	t = 1100°C, τ = 1 h 30 min, p = 0.2–0.14 Pa	Cr_5Al_8, Cr_4Al_9, Al_2O_3
30	20	50	t = 1000°C, τ = 3 h, p = 0.2–0.14 Pa	Cr_4Al_9, $CrAl_4$, Al_2O_3

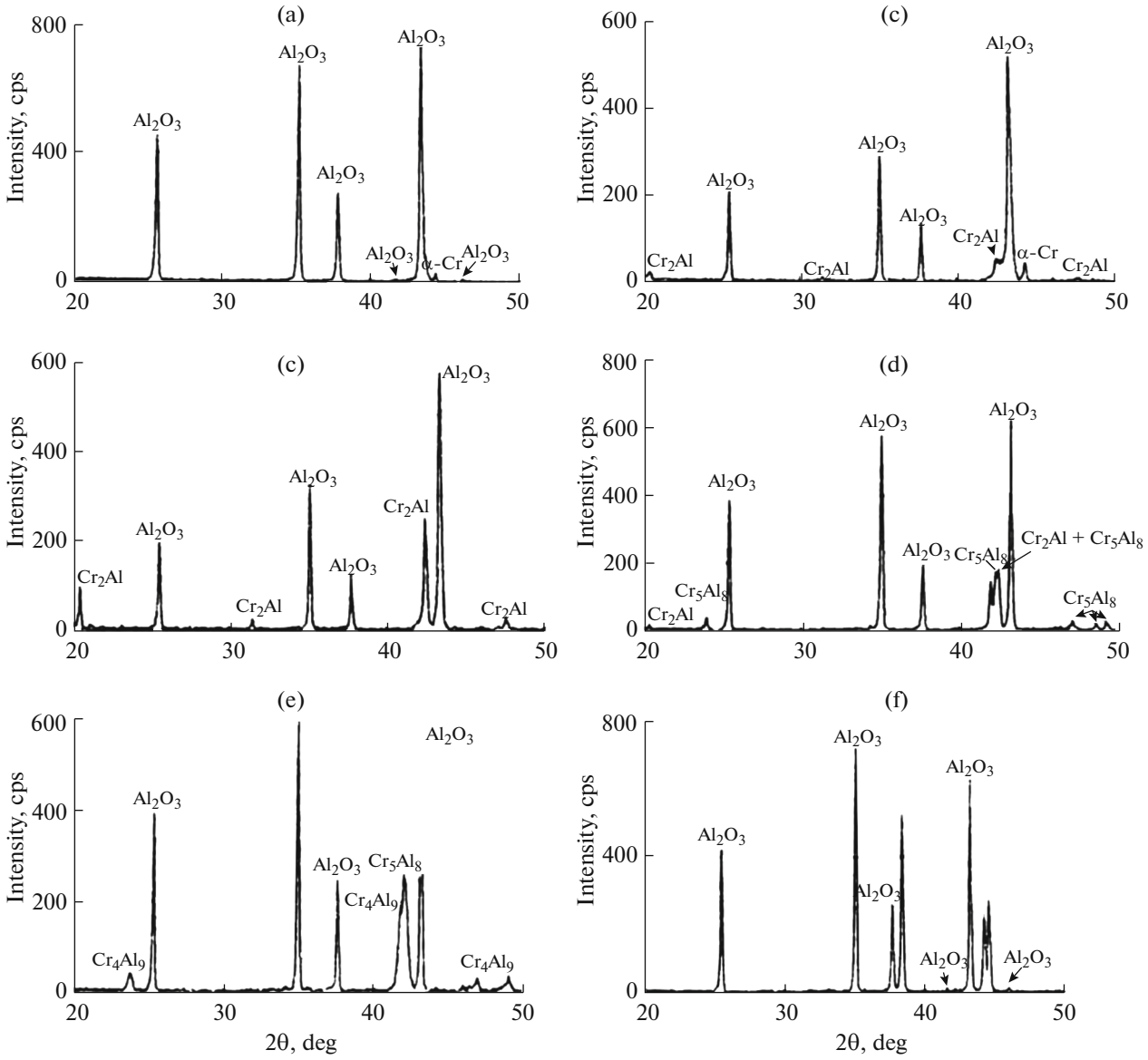

Fig. 1. Fragments of the X-ray diffraction patterns of the mixtures containing Al (wt %): (a) 4, (b) 8, (c) 12, (d) (18), (e) 24, and (f) 30.

X-ray diffraction pattern portions with the most intense lines of the phases under study.

An analysis of the diffraction patterns shows that the phase composition of the annealed mixtures almost coincides with the composition that can be determined on the base of the Cr–Al phase diagram (Fig. 3). Identification of phases α-Cr (in mixtures with 4 and 8% Al) and Cr_2Al (in mixtures with 8-to-18% Al) is not difficult, since the number of lines completely corresponds to the set of interplanar spacing for these phases.

The diffraction pattern of the mixture with 30% Al has the lines that do not belong to Cr_2Al, Cr_5Al_8, and Cr_4Al_9. These lines are most likely to belong to $CrAl_4$, according to the Cr–Al phase diagram in this concentration range.

For the mixture with 4% Al, we determined the lattice parameter of pure chromium in the initial unannealed mixture and the α-Cr solid solution in the annealed mixture (Fig. 4). The lattice parameter was determined by the maxima of $K\alpha_1$ chromium lines (*hkl*: 111, 200, 211, 220, 310, and 222) by the graphic approximation method using the Nelson–Riley extrapolation function

$$f(\theta) = \frac{1}{2}\left(\frac{\cos^2\theta}{\sin\theta} + \frac{\cos^2\theta}{\theta}\right).$$

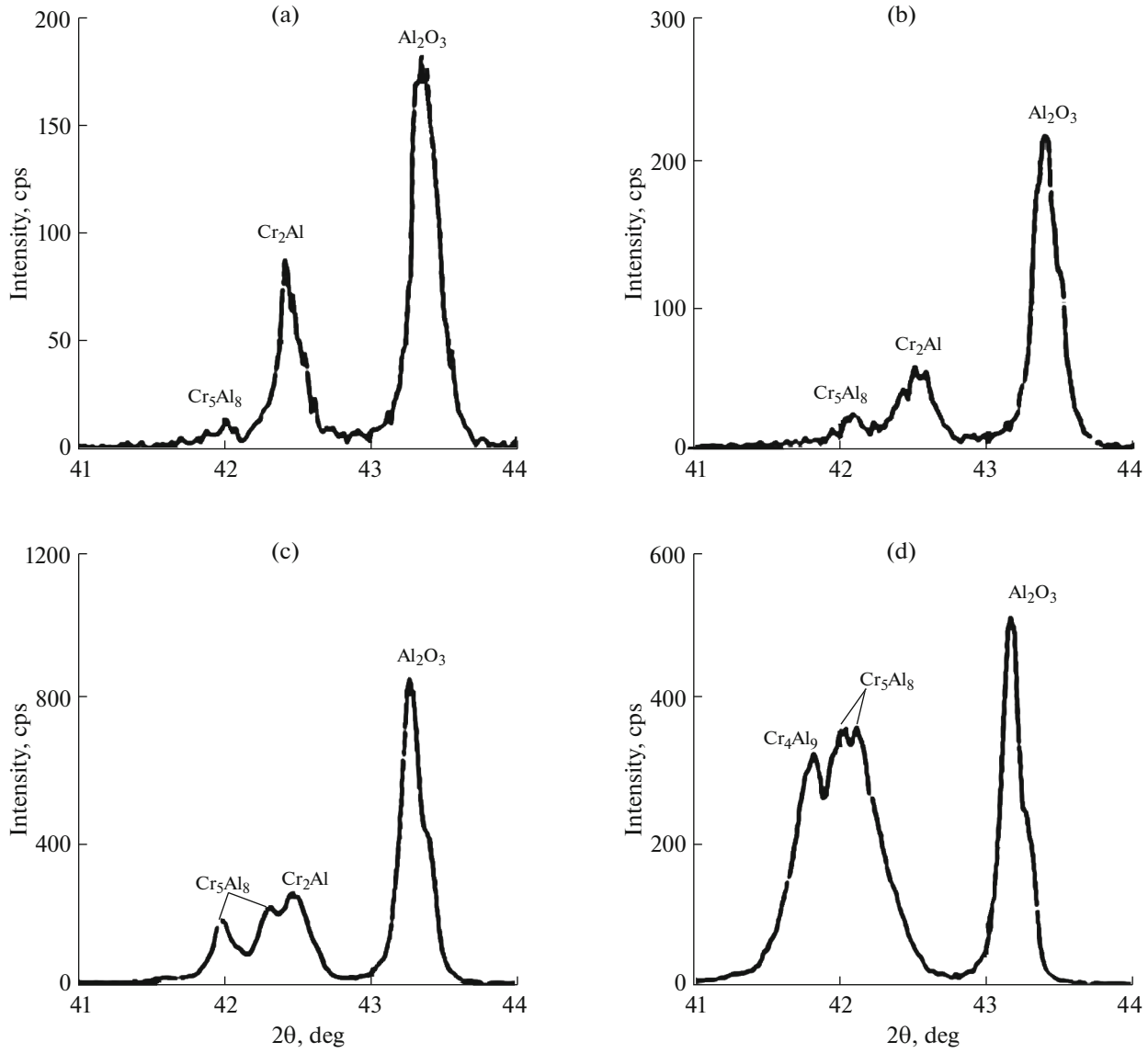

Fig. 2. Fragments of the X-ray diffraction patterns having the most intense peaks in mixtures containing Al (wt %): (a) 12, (b) 15, (c) 18, and (d) (24).

As was expected, the α-Cr lattice parameter is larger than the lattice parameter of pure chromium, since aluminum atoms dissolved in chromium (substitutional atoms) have a larger atomic radius than chromium atoms, $r_{atAl} = 0.143$ nm and $r_{atCr} = 0.128$ nm. It is interesting to note that the chromium lattice parameter coincides with the tabular value to the fifth decimal place and is $\alpha_{Cr} = 0.28347$ nm. The measurements were carried out at room temperature $T = 22–23$°C.

In summary, we note that the powder mixtures with aluminum contents from 12 to 18% have the same phase composition (Cr_2Al, Cr_5Al_8, Al_2O_3) with a variable proportion of the contents of Cr_2Al and Cr_5Al_8.

Thus, we can expect that the aluminum activity in these mixtures is constant due to the equality of the chemical potentials in the binary equilibrium heterogeneous systems (Cr_2Al, Cr_5Al_8). Therefore, the coating obtained in these mixtures with the same conditions should have the same aluminum concentration in the exterior zone.

Thus, the sources of aluminum in the powder mixtures used in vacuum chromoaluminizing are the following phases: the solid solution of aluminum in α-Cr, Cr_2Al, Cr_5Al_8, and Cr_4Al_9.

These phases are formed as a result of high-temperature aluminizing of chromium particles.

In the powder mixtures containing (wt %) 4 Al, 40 Cr, and 56 Al_2O_3 and 8 Al, 40 Cr, and 52 Al_2O_3, aluminum and chromium are in proportions (wt %) 9 Al, 91 Cr and 16.64 Al, 83.36 Cr, respectively. At these

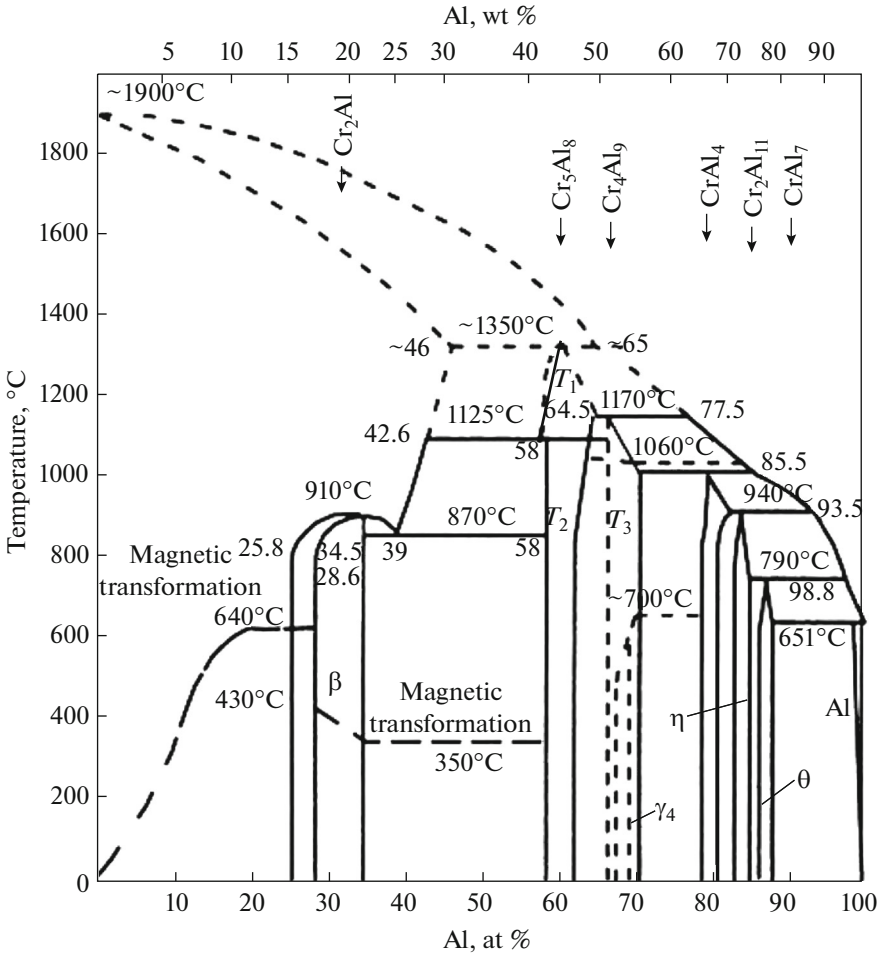

Fig. 3. Cr–Al phase diagram [4].

proportions of elements, only the Cr_2Al intermetallic compound can be expected. The existence of Cr_5Al_8, Cr_4Al_9, and α-Cr indicates a nonuniform distribution of particles in a powder mixture when chromium intermetallic compounds form as a result of contacting chromium and aluminum particles taken in the proportion 20–55 wt % Al and 45–80 wt % Cr; in this case, a significant part of chromium particles in the powder mixture exists as the solid solution of aluminum in chromium. Thus, the intermetallic compounds Cr_2Al, Cr_5Al_8, and Cr_4Al_9 are the main sources of aluminum and supply it to the part surfaces.

The phase composition of the annealed mixtures coincides with the composition determined from the Cr–Al phase diagram. This indicates that the aluminum evaporation during annealing of the mixture in vacuum is insignificant.

To obtain a long life of the coatings operating at temperatures of 1100–1150°C, high-temperature metals, such as tantalum, tungsten, and rhenium, are introduced into the protective layer composition along with chromium and aluminum [5–7]. In addition,

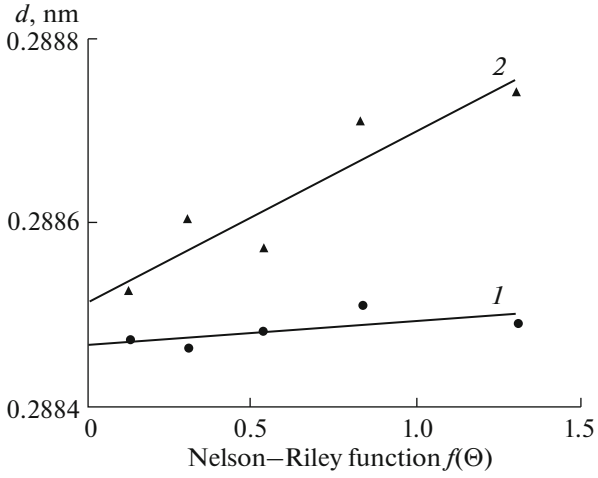

Fig. 4. Determination of the chromium lattice parameter for the mixture containing 4% Al using the Nelson–Riley function: (*1*) unannealed mixture and (*2*) annealed mixture.

Table 2. Chemical composition of the deposited coating sublayer

No.	Alloy for coating	Element contents in coating, wt %					
		Ni	Cr	Ta	W	A1	Y
1	NiCrTaAlY	64.7	17.3	9.4	–	7.8	0.5
2	NiCrTaWAlY	64.3	15.8	5.7	3.7	9.5	1.0
3	NiCrTaY	77.5	14.1	8.4	–	–	–
4	NiCrWAlY	64.5	16.7	–	10.8	7.5	0.5
5	NiCrAlY	63.8	28.7	–	–	7.5	–
6	NiCrAlY	77.3	14.5	–	–	8.2	–

microalloying of the coatings with rare-earth metals is quite effective [8–10]. The combined diffusion–condensation coatings thus formed reliably protect the external and internal surfaces of cooled gas turbine blades in turbomachines.

We tested eight variants of coatings on the ZhS32 alloy for cyclic high-temperature strength: two variants of diffusion coatings, namely, one-stage CrAlY coating obtained as a result of chromoaluminizing in a mixture with a low aluminum activity and two-stage combined coating (NiCrY + CrAlY), and six variants of combined coatings with condensation sublayers of various compositions with almost the same thicknesses.

To study the influence of the chemical composition of the condensation sublayer deposited by vacuum–plasma method on a MAP-1 setup on the cyclic heat resistance of the combined coating, we used the base composition of the NiCrAlY sublayer, (wt %) 15–17 Cr, 7.5–9.5 Al, 0.5–1.5 Y, and Ni for balance.

We studied six variants of the sublayers, the compositions of which differed from the base composition in the tantalum, tungsten, chromium, and aluminum content.

Table 2 gives the chemical compositions of the deposited sublayers of each of the variants. The first variant contains 3–10 wt % tantalum, unlike the base composition; in the second variant, part of tantalum is replaced with tungsten so that the summary contents of tantalum and tungsten almost coincides with the tantalum content in the first case; the third variant contains tantalum and aluminum is absent; the fourth variant differs from the base composition in 10–11 wt % tungsten; in the fifth variant, the chromium content is increased; and the sixth variant is the base.

The cathodes for the deposition of alloy coatings (ACs) were chosen with the aim to study the relative influence of the sublayer elements (Ta, W, Cr, Al) on the formation and the high-temperature strength of the combined coatings at the same sublayer thickness.

The coating was deposited in the following three stages.

At the first stage, ZhS32 alloy samples were coated with sublayers of various compositions and nearly the same thicknesses (about 30 μm at a deposition time of 1.5 h) on the MAP setup.

At the second stage, an aluminide coating was formed on the alloy with a deposited sublayer by powder chromoaluminizing in vacuum. The process was performed in a powder mixture with a low aluminum activity containing (wt %) 4 Al, 40 Cr, 5 NiY alloy, 0.4 NH_4Cl, 51 Al_2O_3 at a temperature of 1200°C for 30 min in vacuum.

The final stage of formation of the coating was the thermovacuum treatment (TVT) of the alloy with the coating at a temperature $T = 1210$°C for 1 h 15 min.

The chemical composition and the thickness of the obtained combined coatings with various compositions of the condensation sublayer are given in Table 3, which also lists the compositions and the thicknesses of the diffusion coatings on the ZhS32 alloy, namely, two-stage combined (NiCrY + CrAlY) coating and one-stage CrAlY coating obtained upon chromoaluminizing of the alloy. The chemical composition of the exterior zone of the coating was determined by electron probe microanalysis using a Stereoscan S-600 electron microscope with a Link microanalyzer by electron-beam scanning over the area 15 × 15 μm.

An analysis of the obtained data shows that the sublayer composition in the considered variants does not influence the summary coating thickness, which is about 35–85 μm. The thickness of the diffusion combined coating was 75–80 μm.

Cyclic high-temperature strength tests were performed at a temperature of 1100°C for 350 h. The cycle included heating to a temperature of 1100°C, holding of a sample at 1100°C for 2 h, and cooling in air within 20 min.

The weighting of samples without crucibles was carried out accurate to 0.1 mg after 2, 5, 10, and 20 cycles and, then, every 10 cycles. The test samples were 18 × 12 × 2-mm rectangular plates.

The processing of the experimental data on the cyclic high-temperature strength of the alloys and the coatings was performed using a program written with Turbo-Pascal 5.0. The initial data for operating the program were the geometric sizes and the current values of the sample masses during tests. The experimen-

Table 3. Chemical compositions and coating thicknesses on the ZhS32 alloy

No.	Coating	Element contents, wt %					h_{subl}, μm	h_{coat}, μm
		Al	Cr	Co	Ta	W		
1	NiCrTaAlY + CrAlY	16.3	7.8	4.2	2.3	3.9	30	80–90
2	NiCrTaWAlY + CrAlY	16.8	7.5	5.3	1.4	3.5	20	90–95
3	NiCrTaY + CrAlY	17.3	7.4	3.0	0.2	3.5	27	80–90
4	NiCrWAlY + CrAlY	16.7	7.0	3.4	1.0	10.0	30	90–95
5	NiCrAlY + CrAlY	16.6	10.6	3.9	2.2	1.9	35	90–100
6	NiCrAlY + CrAlY	16.2	7.6	3.5	0.8	4.0	30	85–90
7	CrAlY	16.3	7.6	7.6	0.8	6.2	–	90–100
8	NiCrY + CrAlY	17.5	6.3	7.5	1.3	2.9	–	75–80

Table 4. Cyclic oxidation constants of the coatings on the ZhS32 alloy

Coating	$k_1^{0.5}$	k_2	k_a	W_1	
				200 h	350 h
NiCrTaWAlY (20) + CrAlY	0.060	0.003	0.09	1.10	1.52
NiCrTaAlY + CrAlY	0.064	0.003	0.09	1.16	1.60
NiCrTaY + CrAlY	0.111	0.007	0.18	2.13	2.99
NiCrAlY + CrAlY	0.110	0.007	0.18	2.13	3.01
NiCrAlY + CrAlY	0.121	0.008	0.20	2.38	3.38
NiCrWAlY + CrAlY	0.179	0. 013	0.31	3.57	5.1
CrAlY	0.387	0.038	0.77	8.40	12.41
NiCrY + CrAlY	0.575	0.060	1.18	12.78	19.03

tal data on the change in the specific sample mass were approximated using the least squares procedure by the paralinear equation

$$\frac{\Delta m}{S} = (k_1 t)^{0.5} - k_2 t, \quad (1)$$

where $\Delta m/S$ is the change in the specific mass, k_1 is a parabolic constant of the oxide film growth rate, k_2 is the constant that characterizes the cleavage and volatility of the oxide film.

As a result, we calculated paralinear constants k_1 and k_2 and gas corrosion constant k_a,

$$k_a = k_1^{0.5} + 10k_2. \quad (2)$$

Equation (1) describes the linear second-order regression model, in which coefficients k_1 and k_2 are parameters. The approximation of the experimental data allows the calculation of coefficients k_1 and k_2 using the least squares procedure and, correspondingly, the calculation of the gas corrosion parameter k_a, which is unambiguously related to the specific content of metal transformed to the oxide by the linear dependence $W_{Me} = W_1$. Coefficient 10 in Eq. (2) was obtained empirically. The values of parameter k_a allow us to range the alloys and the coatings with respect to their resistance to the cyclic oxidation.

The solution of the differential equations of the mass balance upon cyclic oxidation enables the calculation of specific mass of metal W_1 transformed to the oxide and the specific mass of the oxide retained on the sample W_2 for each time.

The values of W_1 and W_2 were calculated assuming that the oxide α-Al_2O_3 film was formed on all coatings over the entire oxidation time. Because of this, constant a equal to the ratio of the masses of aluminum and oxygen in Al_2O_3 was taken to be $a = 1.125$.

Table 4 presents the results of calculating cyclic oxidation constants k_1, k_2, gas corrosion parameter k_a, and the value of W_1 for testing the coatings on the ZhS32 alloy for 200 and 350 h.

The results of calculating gas corrosion parameter k_a show that its value is dependent on a number of experimental points and increases with the test time. This can be related to a deviation of the experimental data from the paralinear dependence or to the "end" effect. This effect is related to the fact that, at the sample ends with combined coatings, there was no sublayer deposited, the coating was diffusion and was oxidized more intensively. The deviation from the para-

Table 5. Gas corrosion parameter k_a for the coatings on the ZhS32 alloy

Coating	Number of cycles, N			
	115	133	154	175
Combined				
NiCrTaWAlY + CrAlY	0.06	0.07	0.08	0.03
NiCrTaAlY + CrAlY	0.07	0.08	0.08	0.09
NiCrAlY + CrAlY	0.11	0.12	0.14	0.18
NiCrTaY + CrAlY	0.14	0.16	0.16	0.18
NiCrAlY + CrAlY	0.13	0.15	0.18	0.20
NiCrWAlY + CrAlY	0.19	0.22	0.25	0.31
Diffusion				
CrAlY	0.57	0.63	0.66	0.77
NiCrY + CrAlY	0.72	0.82	0.97	1.18

linear dependence can be due to a change in the oxidation kinetics, i.e., the formation of other oxides, for example, spinels $NiAl_2O_4$, Cr_2O_3 and NiO, along with α-Al_2O_3.

Table 5 gives the values of the gas corrosion parameter for various numbers of cycles and, correspondingly, various test times of the coatings on the ZhS32 alloy.

Figure 5 shows the experimental dependences of the change in the specific mass of the samples on the test time for the combined NiCrTaWAlY (20 μm) + CrAlY coating, the diffusion CrAlY coating on the ZhS32, and the alloy without coating. For each variant of the coatings, the approximating curves described by

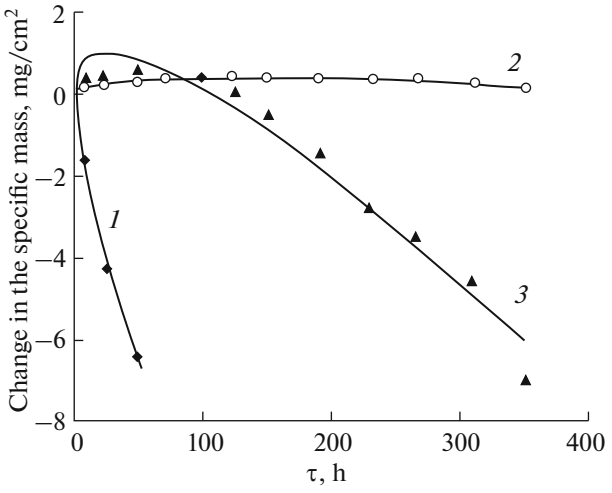

Fig. 5. Change in the sample specific mass vs. the test time for the coatings: (*1*) alloy without coating, (*2*) alloy with NiCrTaWAlY + CrAlY coating, and (*3*) alloy with CrAlY coating.

dependence (1) are presented. The experimental data adequately agree with the paralinear model.

The data shown in Fig. 5 demonstrate a low high-temperature cyclic strength of the ZhS32 alloy at 1100°C. Each of the considered coatings substantially increases the resistance of the alloy to high-temperature cyclic oxidation. In addition, curves *2* and *3* in Fig. 5 show the advantage of the combined coatings in the high-temperature strength as compared to the diffusion coatings. The existence of a 20-μm-thick NiCrTaWAlY sublayer in the combined NiCrTaWAlY (20 μm) + CrAlY coating leads to a noticeable increase in the protective properties as compared to the diffusion CrAlY coating without the sublayer.

The combined coatings with a 30-μm-thick NiCrTaAlY sublayer and a 20-μm-thick NiCrTaWAlY sublayer have the best high-temperature cyclic strength among all considered coating variants. Their gas corrosion parameters are 0.06–0.09 mg/cm^2 h and $k_a < 0.1$, and the coating exhibits a high high-temperature strength at 1100°C.

All other coatings under study have a good high-temperature strength at 1100°C.

The coating with a NiCrWAlY sublayer has the highest gas corrosion parameter k_a = 0.2–0.3 mg/cm^2 h among all variants of the combined coatings on the ZhS32 alloy. Based on this fact, we can conclude that the introduction of a large amount of tungsten (of ~10 wt %) into the deposited sublayer of the combined coating degrades the high-temperature strength of the coating, and the NiCrTaWAlY + CrAlY coating containing 4% tungsten in the sublayer exhibits a high high-temperature strength.

Figure 6 shows the experimental dependences of the change in the specific masses of the samples on the test time and the calculated time dependences for the

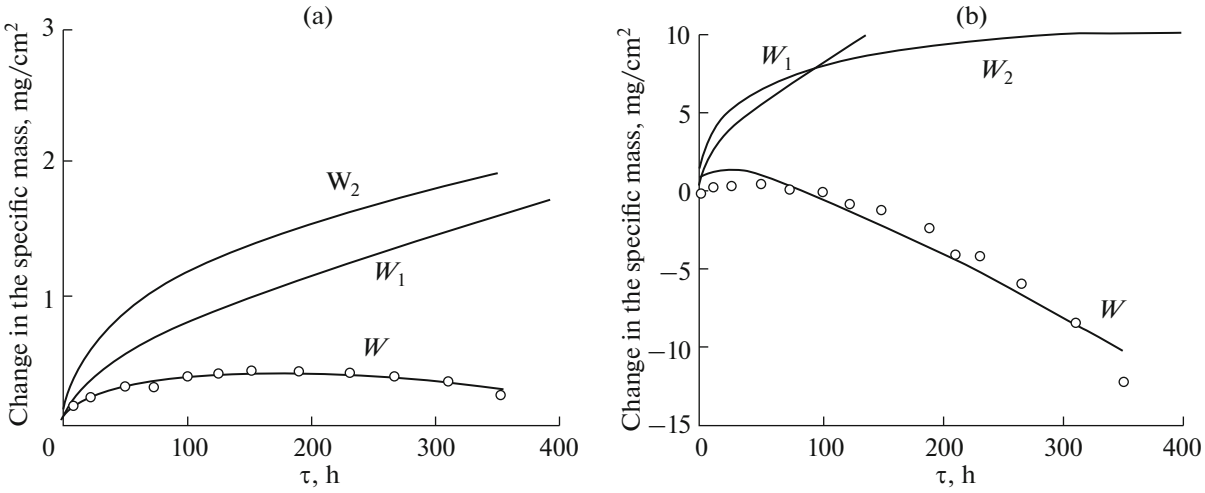

Fig. 6. Experimental dependence of the change in the specific sample mass on the test time and the calculated values of W, W_1, and W_2 for coatings (a) NiCrTaAlY + CrAlY and (b) NiCrY + CrAlY.

specific mass of metal W_1 transformed to the oxide and the specific masses of the oxide retained on the sample W_2 for the combined NiCrTaAlY + CrAlY coating (Fig. 6a) and the diffusion NiCrY + CrAlY coating (Fig. 6b). The mutual change in the dependences $W_1 = f(t)$, $W_2 = \varphi(t)$, and $W = \psi(t)$, where $W =$ the specific mass of the samples during the tests, corresponds to the mass balance equation

$$W = W_2 - W_1. \quad (3)$$

According to this relationship for the combined coating with the NiCrTaAlY sublayer, the value of W is positive over entire time interval of tests, and the specific mass W_2 of the α-Al_2O_3 oxide retained on the sample is larger than the specific mass W_1 of aluminum consumed for the oxidation. Such a relation between W_2 and W_1 is characteristic of two combined coatings, namely, NiCrTaWAlY (20 μm) + CrAlY and NiCrTaAlY + CrAlY. For all other coatings, the curves of the dependence of the specific mass on time intersect the abscissa axis at the time when the values W_2 and W_1 become the same. Then, the value of W becomes negative since $W_2 < W_1$. This moment comes earlier for the diffusion coatings than for the combined coatings.

The data given in Table 4 confirm the unambiguous dependence of gas corrosion parameter k_a on the specific content W_1 of the metal transformed to the oxide. After 350 h tests for the high-temperature strength of the coating on the ZhS32 alloy, it was found that the diffusion coatings completely exhaust their protective properties, and there are no coatings. The alloy surface is the nickel-based γ-solid solution. The β phase is also retained in the structure of the combined coatings with a 30-μm-thick NiCrTaAlY sublayer and a 20-μm-thick NiCrTaWAlY sublayer. The base of the structures of all other combined coatings is the γ′-phase with elements of the γ-solid solution on the surface and in the internal zone.

Judging on the microstructure, we cannot say after the tests that the coating with the NiCrWAlY sublayer has the worst high-temperature strength among all the combined coatings.

An analysis of the obtained data enables us to make the following conclusions:

(1) Any of the considered aluminide coatings substantially improves the high-temperature cyclic strength of the ZhS32 alloy, for which $k_a > 10$ mg/cm^2 h; according to the Barret and Lowell classification, this alloy has a low high-temperature strength at 1100°C.

(2) The high-temperature cyclic strength of any of the considered variants of the combined coatings is higher than that of the diffusion coatings: the gas corrosion parameter of the combined coatings on the ZhS32 alloy is not higher than 0.3 mg/cm^2 h, and it is 0.6 mg/cm^2 h for the diffusion coating considered in this work.

(3) Introduction of (9–10)% tantalum unambiguously increases the high-temperature strength; judging on the value of gas corrosion parameter k_a, the combined coatings containing tantalum in the sublayer are preferable as compared to other coatings.

(4) The combined coatings with a 30-μm-thick NiCrTaAlY sublayer and a 20-μm-thick NiCrTaWAlY sublayer have the best high-temperature cyclic strength among all coating variants under study.

REFERENCES

1. N. V. Abraimov and Yu. S. Eliseev, *Chemothermal Treatment of High-Temperature Steels and Alloys* (Intermet Inzhiniring, Moscow, 2001).

2. E. N. Kablov, *Cast Blades of Gas-Turbine Engines (Alloys, Technologies, and Coatings)* (Nauka, Moscow, 2006).

3. R. D. Jakson, M. P. Taylor, H. E. Evans, and X. H. Li, "Oxidation study of an EB-PVD MCrAlY thermal barrier coating system," Oxid. Met. **76** (3–4), (2011).

4. *Phase Diagrams of Binary Metallic Systems: A Handbook*, Ed. by N. P. Lyakishev (Mashinostroenie, Moscow, 1999), Vol. 3, Book 2.

5. S. A. Muboyadzhan, V. P. Lesnikov, and V. P. Kuznetsov, *Combined Protective Coatings of Turbine Blades of Aviation GTE* (Kvist, Yekaterinburg, 2008).

6. M. P. Taylor, N. E. Evans, S. Gray, and J. R. Nickolls, "Chromia forming thermal barrier coating system," Mater. Corros. **62** (7), 668–673 (2011).

7. A. Pat, D. Oquab, E. Pere, A. Raffaitin, and D. Monecau, "Beneficial effect of Pt and pre-oxidation behavior of an Ni Co Cr Al Y Ta band-coating for thermal barrier coating systems," Oxid. Met. **75**, 247–279 (2011).

8. N. A. Zaitsev, A. V. Logunov, A. A. Shatul'skii, and Yu. N. Shmotin, "A complex determination of the diffusion coefficients of doping elements in high-temperature nickel superalloys and the deposition of polyfunctional multilayer protective coatings," Materialoved., No. 9, 3–10 (2012).

9. H. Guo, T. Zhang, S. Wang, and S. Gong, "Effect of Dy on oxide scale adhesion of coating at 1200°C," Corrosion Science **53**, 2228–2232 (2011).

10. M. Mansumoto, K. Aoyama, H. Matsubara, K. Takayama, T. Banno, Y. Kagiya, and Y. Sugita, "Thermal conductivity and phase stability of plasma sprayed ZrO_2–Y_2O_3–La_2O_2 coatings," Surf. Coat. Techn. **94**, 31–35 (2005).

11. Yu. S. Eliseev, A. M. Dushkin, Yu. P. Shkretov, and N. V. Abraimov, "Method of depositing coatings on high-temperature alloys," RF Patent 2184797, Bull. Izobret., No. 19 (2002).

Translated by Yu. Ryzhkov